ACS APPLIED MATERIALS & INTERFACES

Research Article

www.acsami.org

Ecofriendly and Nonvacuum Electrostatic Spray-Assisted Vapor Deposition of Cu(In,Ga)(S,Se)$_2$ Thin Film Solar Cells

Md. Anower Hossain,[‡] Mingqing Wang,[‡] and Kwang-Leong Choy*

UCL Institute for Materials Discovery, University College London (UCL), Room 107, Roberts Building, Malet Place, London WC1E 7JE, United Kingdom

Supporting Information

ABSTRACT: Chalcopyrite Cu(In,Ga)(S,Se)$_2$ (CIGSSe) thin films have been deposited by a novel, nonvacuum, and cost-effective electrostatic spray-assisted vapor deposition (ESAVD) method. The generation of a fine aerosol of precursor solution, and their controlled deposition onto a molybdenum substrate, results in adherent, dense, and uniform Cu(In,Ga)S$_2$ (CIGS) films. This is an essential tool to keep the interfacial area of thin film solar cells to a minimum value for efficient charge separation as it helps to achieve the desired surface smoothness uniformity for subsequent cadmium sulfide and window layer deposition. This nonvacuum aerosol based approach for making the CIGSSe film uses environmentally benign precursor solution, and it is cheaper for producing solar cells than that of the vacuum-based thin film solar technology. An optimized CIGSSe thin film solar cell with a device configuration of molybdenum-coated soda-lime glass substrate/CIGSSe/CdS/i-ZnO/AZO shows the photovoltaic (j–V) characteristics of V_{oc} = 0.518 V, j_{sc} = 28.79 mA cm^{-2}, fill factor = 64.02%, and a promising power conversion efficiency of η = 9.55% under simulated AM 1.5 100 mW cm^{-2} illuminations, without the use of an antireflection layer. This demonstrates the potential of ESAVD deposition as a promising alternative approach for making thin film CIGSSe solar cells at a lower cost.

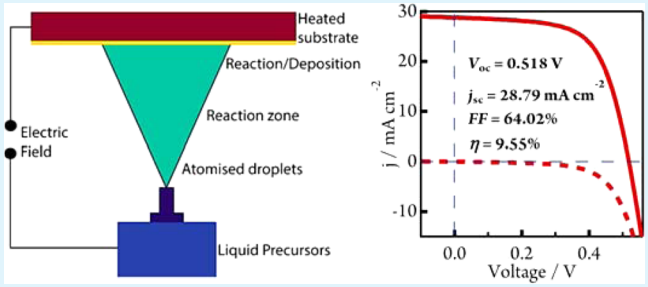

KEYWORDS: *Cu(In,Ga)(S,Se)$_2$, ESAVD deposition, selenization, thin film, solar cells*

1. INTRODUCTION

Chalcopyrite Cu(In,Ga)Se$_2$ (CIGS) thin film solar cells are advantageous over conventional crystalline silicon solar cells in terms of materials processing and the associated cost of production with respect to crystalline silicon solar cells. Its tunable optical properties (band gap of 1.05–1.5 eV) and excellent light harvesting characteristics (absorption coefficient of 10^5 cm^{-1}) allow low usage of precursor materials in order to obtain light harvesting efficiency of close to unity. The research on CIGS thin films and their decent efficiency solar cells leads to the discovery of several emerging light absorbing materials, such as kesterite Cu$_2$ZnSnSe$_4$,[1,2] cadmium telluride (CdTe),[3,4] and lead sulfide (PbS) quantum dots,[5] which have all shown their potential in the conversion of solar energy into electricity at low cost.

While research on CIGS solar cell began decades ago, efforts have mostly focused on the optimization of vacuum-based thin films which has recently resulted in an unprecedented power conversion efficiency (PCE) of 21.7% among all thin film solar cells including CdTe (21.4%) and amorphous silicon (10.5%).[3,6] The vacuum methods, such as multistage coevaporation/sputtering processes, are well-optimized for industrial production lines; however, they are costly because of expensive instrumentation and use of sophisticated vacuum systems.[7−9] It is also challenging to maintain compositional uniformity for large area CIGS films and a H$_2$Se gas treatment step is often required, making the CIGS solar cells vulnerable in terms of associated cost and safety in production.[7,10,11] Therefore, it is crucially important to prepare and optimize CIGS thin films by nonvacuum methods so that solar cells can be prepared more cheaply than the existing vacuum methods.

Significant effort has been invested into preparing low-cost CIGS films using nonvacuum approaches, including spin-coating,[12−19] spray-pyrolysis,[20−24] electrodeposition,[25] and electrostatic spray-assisted vapor deposition (ESAVD).[26−28] These techniques mostly use a molecular precursor solution consisting of either precursors containing sources of copper (Cu), indium (In), and gallium (Ga) with nonmetallic sulfur (S) and selenium (Se) or presynthesized nanoparticles. These solution-based approaches allow selected precursor materials to be prepared into a CIGS absorber film and have similar potential to those of vacuum methods. Among these, the CIGS film prepared by nonvacuum hydrazine (N$_2$H$_4$)-based molecular precursor solution led to the highest 15.2% efficiency solar cells by Mitzi et al.; however, the N$_2$H$_4$ is toxic and explosive in nature, making it undesirable in industrial production lines.[29,30] Solar cells with an efficiency of 8.75% have been reported by dissolving metal oxides into relatively less toxic solvents, such as

Received: July 22, 2015
Accepted: September 21, 2015
Published: September 21, 2015

DOI: 10.1021/acsami.5b06666
ACS Appl. Mater. Interfaces 2015, 7, 22497−22503

carbon disulfide (CS_2), to prepare the molecular precursor materials.[31] These solvents are however also very toxic.

In addition, more than 90% of molecular precursor materials and/or nanoparticles are being wasted on the surrounding area as spin-off material during the spin-coating process,, which is also believed to be less suitable for large scale production. The usage of electrolytes during electrochemical methods is also high which would pose environmental issues for the treatment and safe disposal of the large volumes used for the electrochemical bath, especially with the increasing tighter environmental regulations. Very recently 10.7% efficiency CIGSSe solar cells have been reported by spray-pyrolysis approach using sodium (Na) incorporation and with an antireflection coating.[23] Other nonvacuum precursor solution and nanocrystal inks-based approaches also require postselenization or sulfurization steps, such as spray-pyrolysis-based CIGSSe solar cells have shown an efficiency of 10.54%,[32] electrodeposited CIGS solar cells with efficiency of 10.93%,[33] and the sol−gel approach CIGS solar cell showed 7.04% efficiency.[34] One of the key advantages of the ESAVD approach over other nonvacuum deposition, such as spray pyrolysis, is the use of an electric field during deposition which helps to direct the atomized aerosol chemical precursor to the substrate, thus minimizing the loss of precursor to the surrounding and increase the deposition yield. In fact, the deposition efficiency could be reached close to unity, which is higher than spray pyrolysis, and it is an ideal approach for the large area fabrication of CIGS films.[28,35]

On the basis of these observations, we adopted the ESAVD approach to prepare the CIGS films using environmental friendly precursor materials. A nontoxic alcohol-based solvent, which can dissolve precursor materials was utilized to prepare good quality CIGS films. A postselenization step is carried out to remove any residual solvent from the as-deposited CIGS films and to densify the films so that photovoltaic grade CIGSSe films can be obtained. An optimized CIGSSe solar cell with a device configuration of SLG/Mo/CIGSSe/CdS/i-ZnO/AZO/Ni/Al shows the $j-V$ characteristics of V_{oc} = 0.518 V, j_{sc} = 28.79 mA cm^{-2}, fill factor = 64.02%, and power conversion efficiency (PCE) of η = 9.55% under simulated AM 1.5 100 mW cm^{-2} illuminations without Na incorporation into CIGSSe or an antireflection coating. Our results show the potential of nonvacuum ESAVD for the fabrication of high efficiency CIGSSe thin films using an environmental-friendly, highly reproducible, sustainable, and energy efficient nonvacuum approach with a much lower cost, and there is still plenty of room for further optimization. In overall, the application of nonvacuum ESAVD approach is a very promising way to increase the CIGS deposition rate and to remove the need for expensive high-vacuum systems.

2. EXPERIMENTAL SECTION

Deposition of CIGS Films. The molybdenum (Mo)-coated soda-lime glass (SLG) substrate was sequentially cleaned by sonication in an aqueous solution of 5% Decon D90 solution and DI water, followed by dipping into 10% ammonium hydroxide aqueous solution and drying in nitrogen (N_2) stream prior to the deposition of CIGS films. Metal salt precursors of copper(II) chloride ($CuCl_2$), indium(III) chloride ($InCl_3$), gallium(III) nitrate ($Ga(NO_3)_3$), and thiourea ($SC(NH_2)_2$) with molar concentration within the range 0.2−0.7 M were prepared. The precursor salts were dissolved in a mixture of ethanol−water based solution and atomized and directed to the heated substrate, as schematically shown in Figure 1. Details of the ESAVD method can be found in the literature.[28,35] In brief, an applied voltage of 5−15 kV was used and the precursor flow rate was maintained up to 85 mL/h. The atomizer-to-substrate distance was maintained up to 5 cm. During the ESAVD process, the precursor mixture is atomized to form an aerosol which is charged and subsequently directed toward a heated substrate where it undergoes decomposition and chemical reactions to deposit as a stable solid film of CIGS onto the SLG/Mo substrate. The composition of the CIGS films absorber can be finely controlled by adjusting the ratios of metallic precursors of Cu, In, and Ga in the precursor solution. To prepare the as-deposited CIGS-1, CIGS-2, and CIGS-3 thin films, the precursor ratio of Cu/(In + Ga) was varied from 0.6, 0.75 to 0.78, respectively, while the ratio of Ga/(In + Ga) was maintained at 0.25 for all films. A ratio of Cu/(In + Ga) = 0.62 was found for optimized solar cells.

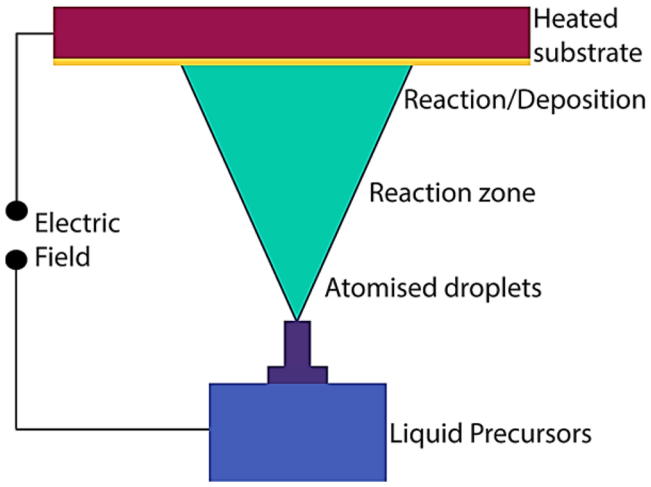

Figure 1. Showing a schematic diagram of electrostatic spray-assisted vapor deposition (ESAVD) method to prepare the as deposited CIGS thin films onto the SLG/Mo substrate.

The as-deposited CIGS films were selenized in a quartz tube furnace (Elite Furnace TSH12/75/750) to allow grain growth and to densify the CIGS films in order to obtain highly crystalline, dense, and pure photovoltaic grade CIGSSe films. A selenium (Se) pellet of 55 mg was taken into a quartz tube at an optimized temperature of 550 °C for 12 min. A preannealing step at 300 °C is required to remove any source of carbon contaminants prior to finally selenize at 550 °C to incorporate selenium into CIGS films and to enhance PCE of the CIGSSe solar cells. The selenization converts as-deposited CIGS films into CIGSSe in which various defect states at grain-boundary regions and surface states are greatly suppressed. After selenization, the CIGSSe films were cooled down to room temperature and transferred immediately into a chemical bath for CdS deposition.

Characterization of Thin Films. Crystal structure of the as-deposited CIGS and postselenized CIGSSe films were characterized by a grazing angle incidence X-ray diffraction (XRD) technique with a Bruker D8 discovery diffractometer using Cu Kα1 radiation (λ = 0.15406 nm). Raman spectroscopy measurement was carried out with a micro-Raman spectrometer (Renishaw inVia Raman Microscope) using a diode-pumped solid-state laser with excitation wavelength of 514 nm. The microstructure of the CIGSSe films was characterized using a variable pressure analytical scanning electron microscope (SEM, JEOL JSM-6480LV). Prior to observation under electron microscopy, a thin Au layer was deposited to prevent charging effects. The elemental analysis of the CIGSSe films was carried out using an Oxford Link system energy-dispersive X-ray spectroscopy (EDS) fitted with the SEM. An X-ray fluorescence analyzer system (Fischer, XRF-250) was utilized to quantify elemental composition of the as-deposited CIGS films.

Fabrication of Solar Cells. An approximately 50 nm thick CdS buffer layer was deposited onto CIGSSe films to obtain the CIGSSe/CdS heterojunction required for the separation of photogenerated charge carriers. While a few alternative buffer layers to the CdS is emerging, CdS is still normally used because of its small lattice

DOI: 10.1021/acsami.5b06666
ACS Appl. Mater. Interfaces 2015, 7, 22497−22503

mismatch with the CIGS films, and it has shown beneficial band energetics with the CIGS and transparent conducting oxide (TCO). In this study, a water bath at 80 °C was utilized as a heat-source for the CIGSSe films containing aqueous solution of 4 mM cadmium acetate hydrate ($Cd(CH_3COO)_2$, 99%), 4 mM ammonium acetate ($NH_4(CH_3COO)$, 99.99%), 2 mM thiourea ($SC(NH_2)_2$, 99%), and 0.4 mL ammonium hydroxide solution (NH_4OH, 28−30% solution). After the deposition of CdS for 10 min, blue colored CIGSSe films were rinsed with DI water and dried in a N_2 stream. Subsequently, an approximately 50 nm thick intrinsic zinc oxide (i-ZnO) film was deposited to protect the CdS buffer layer from plasma damage during the subsequent deposition of aluminum-doped ZnO (AZO) as the TCO layer. The i-ZnO and approximately 600 nm thick AZO layers were deposited by HHV sputtering system with an rf power of 100 W for 15 min and 220 W for 80 min, respectively, to efficiently collect the separated charge carriers. The AZO layer was utilized as TCO because of its more than 90% transparency to the visible solar spectrum, and it has a low electrical resistivity of $<10^{-4}$ Ω cm which allows light to enter into the CIGSSe films and collect the photogenerated charge carrier efficiently before being recombined, respectively.[36,37]

Finally, in order to collect photogenerated charge carriers and transport them with a minimum resistive losses, a patterned bilayer top electrode of Ni/Al (75 nm/400 nm) was thermally evaporated onto the above electrodes using a HHV thermal evaporation system.[36] Subsequently, they were mechanically scribed to define the active area of individual pixel solar cells to be 0.15 cm^2. Solder wire containing 60% tin and 40% lead was deposited onto Mo substrate to make a better contact with measuring cables during device characterization.

Characterization of Solar Cells. A solar simulator (Oriel Sol 1A) was utilized to measure photovoltaic, $j-V$ characteristics of the CIGSSe solar cells under simulated AM 1.5 100 mW cm^{-2} illumination using a Keithley Source (2400) meter and Oriel IV test station software package. The solar simulator was equipped with a 500 W xenon lamp and the light intensity was calibrated using a silicon (Si) reference solar cell (Oriel instruments). External quantum efficiency (EQE) spectra were obtained using a Spequest quantum efficiency photovoltaic system (Rera) equipped with a xenon/quartz lamp. The incident photon flux was determined using the calibrated silicon (Si) and germanium (Ge) photodiodes which allowed us to measure the EQE up to photon wavelength of 1800 nm. The recording of photocurrent spectra were performed using a Photor software package.

3. RESULTS AND DISCUSSION

Structural Characterization of the Thin Films. The thin films were characterized using a grazing angle incidence XRD with an optimized incident angle of 1.25°. As shown in Figure 2, the XRD patterns show characteristic diffraction peaks of CIGSSe-1, CIGSSe-2, CIGSSe-3 and optimized CIGSSe films with various elemental compositions. The XRD patterns of the as-deposited CIGS-1, CIGS-2, and CIGS-3 films show that they consist of crystallites of CIGS (Supporting Information, Figure S1).

The narrow full width at half-maximum (fwhm) and intense XRD peaks suggest the presence of well-crystallized grains in the selenized polycrystalline CIGSSe films (Figure 2). The XRD patterns confirmed the chalcopyrite structure and phase purity of the CIGSSe material. No apparent XRD peaks corresponding to unwanted secondary phases are observed. As all the films consisted of almost equal amounts of Ga (supported by observed same Ga/(In + Ga) ratio of ∼0.25 from the EDS result, Table 1), a shift of the XRD peaks among the CIGSSe films, which occurs due to Ga incorporation and subsequent change of crystal lattice, was not observed.[32] A broad and low intensity peak at $\sim 2\theta = 31°$ for all samples implies the existence of a thin $MoSe_2$ layer formed due to the diffusion of Se^{2-} vapor through as-deposited CIGS films.[38] The

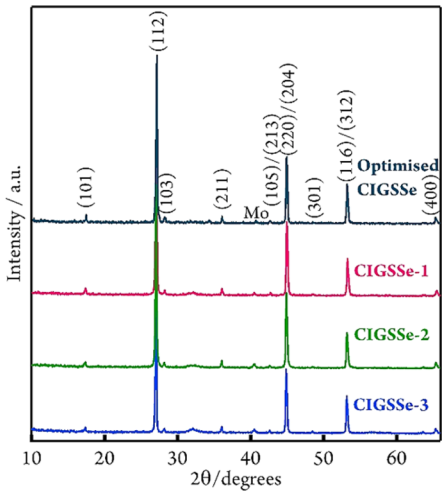

Figure 2. XRD patterns of CIGSSe thin films with various Cu/(In +Ga) ratios fabricated onto Mo-coated SLG substrate. The Cu/(In +Ga) ratio in the CIGSSe-1, CIGSSe-2, CIGSSe-3, and optimized CIGSSe films are observed to be 0.77, 0.79, 0.89, and 0.78, respectively.

absence of XRD peaks corresponding to $Cu_{2-x}Se$ confirms that these CIGSSe films are phase pure.[39]

Morphological Characterization. Figure 3 shows typical morphological characteristics of the optimized CIGSSe films investigated by SEM. The top-view image, as shown in Figure 3a, illustrates that the materials exhibit interconnected large grains of CIGSSe with a size of 0.8−1.5 μm which ultimately forms a dense, thin film. The corresponding cross-sectional image indicates the thickness of the CIGSSe film (Figure 3b) to be an average of 1 μm and covers the entire Mo substrate. Such an interconnected grainy structure and compact CIGSSe film also indicates an improved selenization step when process temperature, time, and amount of selenium, which assists grain growth are considered. As demonstrated by Figure 3b, the dense CIGSSe film may lead to a significantly thin $MoSe_2$ layer onto the Mo substrate because of suppressed diffusion of reactive Se^{2-} through intergrains of the CIGSSe films to reach the substrate. An insignificant variation of grain size of 0.8−1.4, 0.8−1.4, and 0.85−1.6 μm was observed for the CIGSSe-1, CIGSSe-2, and CIGSSe-3 thin films, respectively (Figure S2, Supporting Information).

Compositional Analysis. Compositional analysis of the as-deposited CIGS films was conducted by XRF which shows calculated values of Cu/(In + Ga) as 0.60, 0.75, 0.78, and 0.62 and for Ga/(In + Ga) as 0.24, 0.23, 0.23, and 0.22 for the as-deposited CIGS-1, CIGS-2, CIGS-3, and optimized CIGS films, respectively (Supporting Information, Table S1).

The Cu deficiency is required in the films to eliminate any chance of formation of secondary phases of $Cu_{2-x}S$, $Cu_{2-x}Se$, Cu_3Se_2, and CuSe. However, as shown in Table 1, after selenization, the Cu/(In + Ga) ratio has increased to 0.77, 0.79, 0.89, and 0.78 in the CIGSSe-1, CIGSSe-2, CIGSSe-3, and optimized CIGSSe film, respectively. These values are close to the known optimum value of 0.85 for high efficiency CIGS solar cells. The increase of the Cu/(In + Ga) and Ga/(In + Ga) ratios suggests a loss of In during the selenization step. These Cu-deficient CIGSSe films were utilized to fabricate the solar cells.

Raman Spectroscopy. The crystallographic data alone is not sufficient to accurately determine the phase purity of the

DOI: 10.1021/acsami.5b06666
ACS Appl. Mater. Interfaces 2015, 7, 22497−22503

Table 1. Compositional Study of the CIGSSe Thin Films by EDS Elemental Analysis

thin films	Cu (at %)	In (at %)	Ga (at %)	S (at %)	Se (at %)	Cu/(In + Ga)	Ga/(In + Ga)	Se/(S + Se)
CIGSSe-1	18.65	17.82	6.15	10.56	46.82	0.77	0.25	0.81
CIGSSe-2	16.51	15.85	5.06	13.29	49.29	0.79	0.24	0.78
CIGSSe-3	21.69	18.01	6.26	9.93	44.11	0.89	0.25	0.81
optimized CIGSSe	20.07	18.10	7.44	3.61	50.78	0.78	0.29	0.93

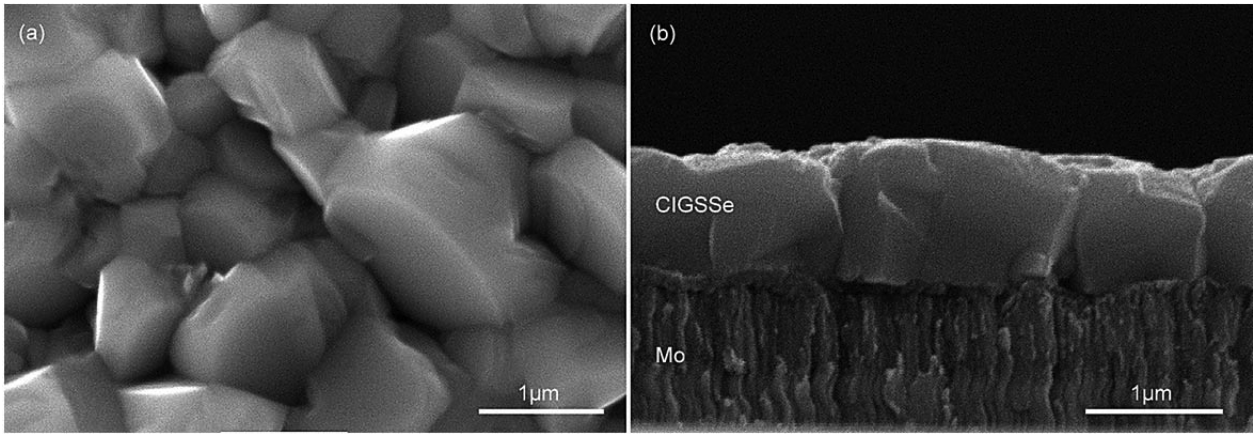

Figure 3. (a) Surface morphology and (b) cross-sectional image of the optimized CIGSSe thin film.

CIGSSe films as they often produce nonstoichiometric phases during selenization where the XRD peaks could overlap in the diffraction patterns of CIGSSe, leading to an incorrect conclusion. Therefore, the films were studied by Raman spectroscopy to correctly probe the insight of the CIGSSe films and deduce whether impurity phases of $Cu_{2-x}Se$, Cu_3Se_2, CuSe, were present in the films, despite the fact that the XRD patterns, as shown in Figure 2, confirmed their absence. The films selenized at 550 °C show the dominant Raman bands of the A_1 mode at 178 cm^{-1} with narrow fwhm and also show mixed $B_{2/E}$ modes at around 218 cm^{-1} (Figure 4).[40,41]

The vibrational mode at around 220−260 cm^{-1} corresponds to a mixed mode of $B_{2/E}$ of Cu-poor CIGSSe films.[42] It also implies that there are no apparent impurity phases of $Cu_{2-x}Se$, CuSe, and Cu_3Se_2 in the CIGSSe films and the films are good quality. The intensities of Raman bands at around 295 cm^{-1} corresponding to CIGS films, and they become insignificant with respect to that of 177 cm^{-1}, corresponding to CIGSSe films, confirming a high Se/S in the films. The Raman spectra do not reveal a broad vibrational mode at around 150 cm^{-1}, implying that there are no apparent order defects of $Cu(In,Ga)_3(S,Se)_5$ or $Cu_2(In,Ga)_4(S,Se)_7$ which tend to occur in Cu-poor CIGS films.[43]

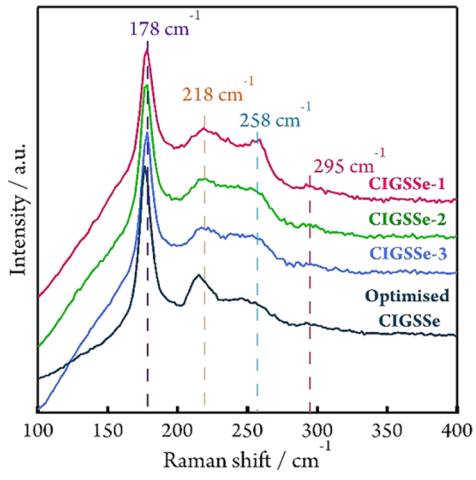

Figure 4. Raman spectra of the CIGSSe thin films deposited onto Mo substrate with various Cu/(In + Ga) ratios.

Photovoltaic *j*−*V* Characteristics. Solar cells were fabricated using CIGSSe thin films with a conventional device structure of SLG/Mo/CIGSSe/CdS/i-ZnO/AZO/Ni/Al. The decent *j*−*V* characteristics of solar cells are tabulated in Table 2,

Table 2. *j*−*V* Characteristics of CIGSSe Solar Cells under Simulated AM 1.5, 100 mW cm^{-2} Illumination

solar cells	V_{oc} (V)	j_{sc} (mA cm^{-2})	FF (%)	η (%)	R_s (Ω cm^2)	R_{sh} (Ω cm^2)
CIGSSe-1	0.540	26.12	63.46	8.95	3.16	264.76
CIGSSe-2	0.549	25.69	53.93	7.61	4.72	120.27
CIGSSe-3	0.475	28.23	41.95	5.62	5.87	89.85
optimized CIGSSe	0.518	28.79	64.02	9.55	2.83	408.95

and the *j*−*V* curves are shown in Figure 5a. As compared with the CIGSSe-2, the efficiency of the solar cells is found to be improved when using the film of CIGSSe-1, which has slightly higher Ga/(In + Ga) = 0.25 and lower Cu/(In + Ga) = 0.77, this may suggest its excellent electronic properties (charge carrier mobilities, densities, etc.). For the CIGSSe-3 film, despite the fairly similar Ga/(In + Ga) ratio of 0.25 with CIGSSe-1, it exhibited poor rectification behavior because of the high value of the Cu/(In + Ga) ratio of 0.89. The optimized solar cell showed the best efficiency of 9.55% with V_{oc} = 0.518 V, j_{sc}= 28.79 mA cm^{-2}, and FF = 64.02%.

The PCE of these solar cells can be improved further by optimizing the thickness of CIGSSe films and using a TCO layer with reduced optical and resistive losses. In general, the V_{oc} value should increase with CIGSSe film thickness, provided that they are pure and crystalline with suppressed trap states for

DOI: 10.1021/acsami.5b06666
ACS Appl. Mater. Interfaces 2015, 7, 22497−22503

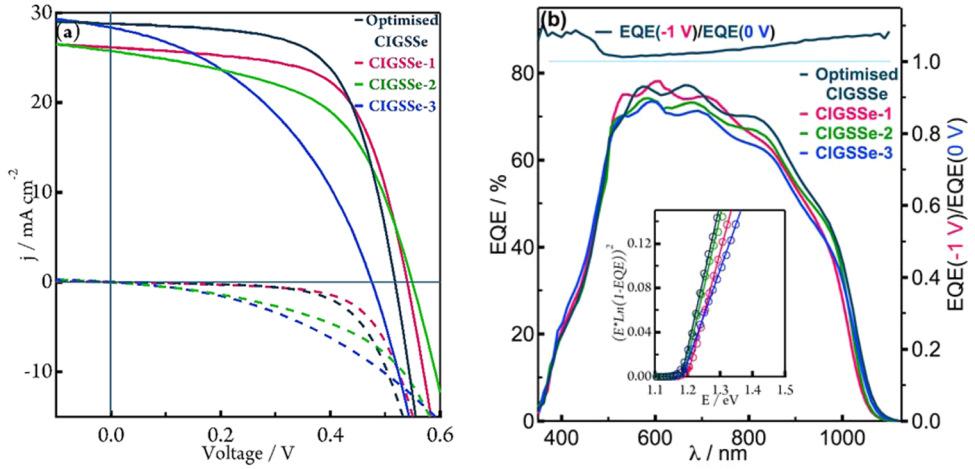

Figure 5. (a) $j-V$ characteristics of CIGSSe thin film solar cells measured under simulated AM 1.5 100 mW cm^{-2} illuminations, (b) the EQE spectra of corresponding solar cells. The inset of part b shows the Tauc-plot using EQE spectra and the approximate band gap values of CIGSSe-1, CIGSSe-2, CIGSSe-3, and optimized CIGSSe films. The top section of part b shows the EQE ratio, [EQE(−1 V)/EQE(0 V)], for the CIGSSe-3 solar cell.

carrier recombination. The fill factor of the optimized solar cells is 64.02%, implying that the CIGSSe/CdS interface needs to be optimized along with reducing series resistance (R_s) and raising shunt resistance (R_{sh}). A much higher PCE of CIGSSe solar cell is expected if these parasitic resistances are reduced to a greater extent.

EQE measurements, as depicted in Figure 5b, show conversion of photons beyond 1100 nm in the solar spectrum. The highest photocurrent response is observed to be approximately 75% for the CIGSSe-1 solar cells. However, this peak EQE is actually much lower than typical vacuum-based solar cells, usually above 90%, suggesting the major loss in j_{sc} could be due to comparatively poor carrier collection efficiency, pronounced recombination, short lifetime of minority carriers resulting from defect states at various interfaces, and insufficiently thick CIGSSe films with low light harvesting efficiency. In addition, the EQE curve of the CIGSSe-3 solar cell is found to be more deficient in the long wavelength region, near the band edge, which indicates a pathway for recombination loss which is deep in the CIGSSe layer, or a shorter minority carrier diffusion length, which limits the carrier collection efficiency. The EQE bias ratio plot, the ratio of EQE measured at −1 and 0 V, [EQE(−1 V)/EQE(0 V)], as shown in the top section of Figure 5b shows an increasing [EQE(−1 V)/EQE(0 V)] ratio with photon wavelength, especially at longer wavelength, suggesting a voltage-dependent collection efficiency which occurs in solar cells with shorter minority carrier diffusion length. Therefore, further improvement of films quality (i.e., larger grain size, passivation of grain boundaries incorporating alkaline materials, and optimizing the heterojunction interfaces) is crucial to obtain enhanced carrier collection efficiency in solar cells.

Provided that the carrier collection is efficient in device, an improvement of j_{sc} is expected by increasing the light harvesting efficiency using a relatively thicker CIGSSe absorber layer that may also prevent the shunting pathways in device. The j_{sc} of the solar cells were relatively lower than that of the reported high efficiency vacuum-based CIGS solar cell (>32 mA cm^{-2}). This is mainly due to the use of a thinner CIGSSe film (average thickness 1 μm), which was much lower than the optimal value (2 μm). In addition, lowering bulk resistance of the different stack layers, i.e., Mo, CIGSSe, CdS, and AZO layers, and improving the charge transport characteristics at these adjacent interfaces, are alternative ways to further improve the j_{sc}. Overall, the $j-V$ characteristic of these solar cells suggest that there are still several paths to improve their efficiency, i.e., photon management by incorporating an antireflection coating to enhance light harvesting efficiency of these solar cells, and consequently increasing their power conversion efficiency. The reduced EQE below a photon wavelength of 500 nm is due to the light absorption by CdS, buffer (i-ZnO), and window (AZO) layers, which can be reduced by using their optimized layer thickness.[44] The reduced EQE in the near-infrared region (1050 nm onward) could also be due to incomplete absorption of incident light by the CIGSSe films and/or due to reflectivity of free-carrier absorption from the AZO contact and various recombination losses in this long wavelength region.[44]

The CIGSSe-3 solar cells showed comparatively lower EQE which could be the result of inefficient charge separation in Cu-rich CIGSSe-3 materials and its heterojunction interface with CdS. The E_g of the CIGSSe-1, CIGSSe-2, and CIGSSe-3 were calculated to be 1.2, 1.19, and 1.18 eV, respectively from the corresponding Tauc-plot of the EQE spectra [inset of Figure 5b]. These are surprisingly similar because of similar Se/(S + Se) ratios of 0.78−0.81 (Table 1). In this context, the optimized CIGSSe solar cells show slightly lower E_g values of approximately 1.15 eV because of a higher Se/(Se + S) ratio of 0.93 (Table 1), implying incorporation of more Se during the selenization step. It is worth noting that a high efficiency coevaporation-based CIGS device requires an approximately 2 μm thick absorbent layer with an E_g values of 1.15−1.18 eV.[45] The wavelength dependent quantum efficiencies for the these solar cells, in the range of 500 to 850 nm, could arise from optical losses from the AZO layer, which requires further studies for better understanding of different stack layers.

Figure 6 shows a cross-sectional SEM image of the optimized CIGSSe solar cell made onto Mo-coated SLG substrate. The CIGSSe film has a thickness of ∼1 μm consisting of large crystal grains of more than 1 μm. There was no void in between the Mo and CIGSSe layers. An amorphous conformal CdS layer of approximately 50 nm thick can be seen on top of the CIGSSe film. The SEM image suggests that the $MoSe_2$ layer, which in generally formed during the selenization step, is actually very thin (Figure 6). We believe that the highly

DOI: 10.1021/acsami.5b06666
ACS Appl. Mater. Interfaces 2015, 7, 22497−22503

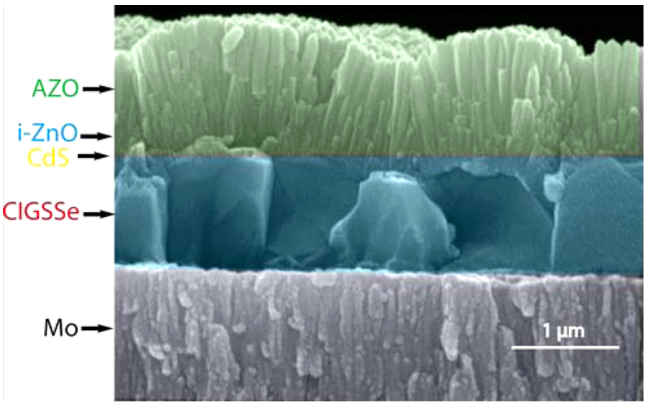

Figure 6. Cross-sectional image of the optimized CIGSSe solar cell with stack layers of Mo, CIGSSe, CdS, i-ZnO, and AZO.

crystalline and pure CIGSSe thin films prepared with environmental friendly precursors, and the cheaper non vacuum ESAVD method, will allow us to fabricate solar cells with promising efficiency in more cost-effective ways. This is very encouraging for further development of alternative low-cost and high throughput nonvacuum processed CIGSSe thin film solar cells.

4. CONCLUSIONS

In summary, CIGSSe thin films have been successfully fabricated using an environmental friendly, nonvacuum ESAVD approach with subsequent selenization. The composition of CIGSSe films was varied using different amounts of precursor solution containing Cu, In, Ga, and S. The as-deposited uniform CIGS films were nanocrystalline and adhered well onto Mo substrates. After the selenization step, they were transformed into highly crystalline CIGSSe thin films. The XRD and Raman study revealed the phase purity of the CIGSSe thin films. The solar cells fabricated with an optimized and highly crystalline CIGSSe films showed power conversion efficiencies of 9.55% under simulated AM1.5 100 mW cm^{-2} solar irradiation. These results show that the ESAVD is a promising approach for the fabrication of cost-effective chalcogenide thin film solar cells.

■ ASSOCIATED CONTENT

Supporting Information

The Supporting Information is available free of charge on the ACS Publications website at DOI: 10.1021/acsami.5b06666.

XRD patterns and composition of the as-deposited CIGS thin films; SEM images of the CIGSSe thin films (PDF)

■ AUTHOR INFORMATION

Corresponding Author

*E-mail: k.choy@ucl.ac.uk.

Author Contributions

‡M.A.H. and M.W. contributed equally.

All authors have given approval to the final version of the manuscript.

Notes

The authors declare no competing financial interest.

■ ACKNOWLEDGMENTS

The authors would like to acknowledge the financial support from the University College London and the European Union's Seventh Framework Programme, Scalenano, FP7/2007-2013 under Grant Agreement Number 284486. We would also like to thank Dr. Charlotte Linfoot for proofreading the manuscript.

■ REFERENCES

(1) Todorov, T. K.; Tang, J.; Bag, S.; Gunawan, O.; Gokmen, T.; Zhu, Y.; Mitzi, D. B. Beyond 11% Efficiency: Characteristics of State-of-the-Art Cu2ZnSn(S,Se)4 Solar Cells. *Adv. Energy Mater.* **2013**, *3*, 34−38.

(2) van Embden, J.; Chesman, A. S. R.; Della Gaspera, E.; Duffy, N. W.; Watkins, S. E.; Jasieniak, J. J. $Cu_2ZnSnS_{4x}Se_{4(1-x)}$ Solar Cells from Polar Nanocrystal Inks. *J. Am. Chem. Soc.* **2014**, *136*, 5237−5240.

(3) Green, M. A.; Emery, K.; Hishikawa, Y.; Warta, W.; Dunlop, E. D. Solar cell efficiency tables (Version 45). *Prog. Photovoltaics* **2015**, *23*, 1−9.

(4) Green, M. A.; Emery, K.; Hishikawa, Y.; Warta, W.; Dunlop, E. D. Solar cell efficiency tables (version 46). *Prog. Photovoltaics* **2015**, *23*, 805−812.

(5) Tang, J.; Kemp, K. W.; Hoogland, S.; Jeong, K. S.; Liu, H.; Levina, L.; Furukawa, M.; Wang, X.; Debnath, R.; Cha, D.; Chou, K. W.; Fischer, A.; Amassian, A.; Asbury, J. B.; Sargent, E. H. Colloidal-quantum-dot photovoltaics using atomic-ligand passivation. *Nat. Mater.* **2011**, *10*, 765−771.

(6) Jackson, P.; Hariskos, D.; Wuerz, R.; Kiowski, O.; Bauer, A.; Friedlmeier, T. M.; Powalla, M. Properties of Cu(In,Ga)Se2 solar cells with new record efficiencies up to 21.7%. *Phys. Status Solidi RRL* **2015**, *9*, 28−31.

(7) Chirila, A.; Reinhard, P.; Pianezzi, F.; Bloesch, P.; Uhl, A. R.; Fella, C.; Kranz, L.; Keller, D.; Gretener, C.; Hagendorfer, H.; Jaeger, D.; Erni, R.; Nishiwaki, S.; Buecheler, S.; Tiwari, A. N. Potassium-induced surface modification of $Cu(In,Ga)Se_2$ thin films for high-efficiency solar cells. *Nat. Mater.* **2012**, *12*, 1107−1111.

(8) Repins, I.; Contreras, M. A.; Egaas, B.; DeHart, C.; Scharf, J.; Perkins, C. L.; To, B.; Noufi, R. 19·9%-efficient $ZnO/CdS/CuInGaSe_2$ solar cell with 81·2% fill factor. *Prog. Photovoltaics* **2008**, *16*, 235−239.

(9) Schleussner, S. M.; Törndahl, T.; Linnarsson, M.; Zimmermann, U.; Wätjen, T.; Edoff, M. Development of gallium gradients in three-stage Cu(In,Ga)Se2 co-evaporation processes. *Prog. Photovoltaics* **2012**, *20*, 284−293.

(10) Liang, H.; Avachat, U.; Liu, W.; van Duren, J.; Le, M. CIGS formation by high temperature selenization of metal precursors in H2Se atmosphere. *Solid-State Electron.* **2012**, *76*, 95−100.

(11) Green, M. A.; Emery, K.; Hishikawa, Y.; Warta, W.; Dunlop, E. D. Solar cell efficiency tables (version 43). *Prog. Photovoltaics* **2014**, *22*, 1−9.

(12) Park, S. J.; Cho, J. W.; Lee, J. K.; Shin, K.; Kim, J.-H.; Min, B. K. Solution processed high band-gap $CuInGaS_2$ thin film for solar cell applications. *Prog. Photovoltaics* **2014**, *22*, 122−128.

(13) Mitzi, D. B.; Yuan, M.; Liu, W.; Kellock, A. J.; Chey, S. J.; Deline, V.; Schrott, A. G. A High-Efficiency Solution-Deposited Thin-Film Photovoltaic Device. *Adv. Mater.* **2008**, *20*, 3657−3662.

(14) Chung, C.-H.; Bob, B.; Lei, B.; Li, S.-H.; Hou, W. W.; Yang, Y. Hydrazine solution-processed $CuIn(Se,S)_2$ thin film solar cells: Secondary phases and grain structure. *Sol. Energy Mater. Sol. Cells* **2013**, *113*, 148−152.

(15) Jeong, S.; Lee, B.-S.; Ahn, S.; Yoon, K.; Seo, Y.-H.; Choi, Y.; Ryu, B.-H. An 8.2% efficient solution-processed CuInSe2 solar cell based on multiphase CuInSe2 nanoparticles. *Energy Environ. Sci.* **2012**, *5*, 7539−7542.

(16) Akhavan, V. A.; Goodfellow, B. W.; Panthani, M. G.; Reid, D. K.; Hellebusch, D. J.; Adachi, T.; Korgel, B. A. Spray-deposited $CuInSe_2$ nanocrystal photovoltaics. *Energy Environ. Sci.* **2010**, *3*, 1600−1606.

(17) Akhavan, V. A.; Harvey, T. B.; Stolle, C. J.; Ostrowski, D. P.; Glaz, M. S.; Goodfellow, B. W.; Panthani, M. G.; Reid, D. K.; Vanden

DOI: 10.1021/acsami.5b06666
ACS Appl. Mater. Interfaces 2015, 7, 22497−22503

Bout, D. A.; Korgel, B. A. Influence of Composition on the Performance of Sintered Cu(In,Ga)Se_2 Nanocrystal Thin-Film Photovoltaic Devices. *ChemSusChem* **2013**, *6*, 481−486.
(18) Kar, M.; Agrawal, R.; Hillhouse, H. W. Formation Pathway of CuInSe2 Nanocrystals for Solar Cells. *J. Am. Chem. Soc.* **2011**, *133*, 17239−17247.
(19) Guo, Q.; Kim, S. J.; Kar, M.; Shafarman, W. N.; Birkmire, R. W.; Stach, E. A.; Agrawal, R.; Hillhouse, H. W. Development of $CuInSe_2$ Nanocrystal and Nanoring Inks for Low-Cost Solar Cells. *Nano Lett.* **2008**, *8*, 2982−2987.
(20) Hossain, M. A.; Tianliang, Z.; Keat, L. K.; Xianglin, L.; Prabhakar, R. R.; Batabyal, S. K. K.; Mhaisalkar, S. G.; Wong, L. H. Synthesis of Cu(In,Ga)(S,Se)2 thin films using an aqueous spray-pyrolysis approach, and their solar cell efficiency of 10.5%. *J. Mater. Chem. A* **2015**, *3*, 4147.
(21) Cai, Y.; Ho, J. C. W.; Batabyal, S. K.; Liu, W.; Sun, Y.; Mhaisalkar, S. G.; Wong, L. H. Nanoparticle-Induced Grain Growth of Carbon-Free Solution-Processed $CuIn(S,Se)_2$ Solar Cell with 6% Efficiency. *ACS Appl. Mater. Interfaces* **2013**, *5*, 1533−1537.
(22) Ho, J. C. W.; Zhang, T.; Lee, K. K.; Batabyal, S. K.; Tok, A. I. Y.; Wong, L. H. Spray Pyrolysis of $CuIn(S,Se)_2$ Solar Cells with 5.9% Efficiency: A Method to Prevent Mo Oxidation in Ambient Atmosphere. *ACS Appl. Mater. Interfaces* **2014**, *6*, 6638−6643.
(23) Septina, W.; Kurihara, M.; Ikeda, S.; Nakajima, Y.; Hirano, T.; Kawasaki, Y.; Harada, T.; Matsumura, M. $Cu(In,Ga)(S,Se)_2$ Thin Film Solar Cell with 10.7% Conversion Efficiency Obtained by Selenization of the Na-Doped Spray-Pyrolyzed Sulfide Precursor Film. *ACS Appl. Mater. Interfaces* **2015**, *7*, 6472−6479.
(24) Harvey, T. B.; Mori, I.; Stolle, C. J.; Bogart, T. D.; Ostrowski, D. P.; Glaz, M. S.; Du, J.; Pernik, D. R.; Akhavan, V. A.; Kesrouani, H.; Vanden Bout, D. A.; Korgel, B. A. Copper Indium Gallium Selenide (CIGS) Photovoltaic Devices Made Using Multistep Selenization of Nanocrystal Films. *ACS Appl. Mater. Interfaces* **2013**, *5*, 9134−9140.
(25) Aksu, S.; Pethe, S.; Kleiman-Shwarsctein, A.; Kundu, S.; Pinarbasi, M. Recent advances in electroplating based CIGS solar cell fabrication. In *Photovoltaic Specialists Conference (PVSC), 2012 38th IEEE*, June 3−8, 2012; pp 003092−003097.
(26) Hou, X.; Choy, K.-L. Synthesis and characteristics of CuInS2 films for photovoltaic application. *Thin Solid Films* **2005**, *480−481*, 13−18.
(27) Liu, J. P.; Choy, K. L.; Placidi, M.; López-García, J.; Saucedo, E.; Colombara, D.; Robert, E. Fabrication and characterization of kesterite Cu2ZnSnS4 thin films deposited by electrostatic spray assisted vapour deposition method. *Phys. Status Solidi A* **2015**, *212*, 135−139.
(28) Wang, M.; Hou, X.; Liu, J.; Choy, K.; Gibson, P.; Salem, E.; Koutsogeorgis, D.; Cranton, W. An alternative non-vacuum and low cost ESAVD method for the deposition of Cu(In,Ga)Se2 absorber layers. *Phys. Status Solidi A* **2015**, *212*, 72−75.
(29) Liu, W.; Mitzi, D. B.; Yuan, M.; Kellock, A. J.; Chey, S. J.; Gunawan, O. 12% Efficiency $CuIn(Se,S)_2$ Photovoltaic Device Prepared Using a Hydrazine Solution Process†. *Chem. Mater.* **2010**, *22*, 1010−1014.
(30) Todorov, T. K.; Gunawan, O.; Gokmen, T.; Mitzi, D. B. Solution-processed Cu(In,Ga)(S,Se)2 absorber yielding a 15.2% efficient solar cell. *Prog. Photovoltaics* **2013**, *21*, 82−87.
(31) Wang, G.; Wang, S.; Cui, Y.; Pan, D. A Novel and Versatile Strategy to Prepare Metal−Organic Molecular Precursor Solutions and Its Application in $Cu(In,Ga)(S,Se)_2$ Solar Cells. *Chem. Mater.* **2012**, *24*, 3993−3997.
(32) Hossain, M. A.; Tianliang, Z.; Keat, L. K.; Xianglin, L.; Prabhakar, R. R.; Batabyal, S. K.; Mhaisalkar, S. G.; Wong, L. H. Synthesis of $Cu(In,Ga)(S,Se)_2$ thin films using an aqueous spray-pyrolysis approach, and their solar cell efficiency of 10.5%. *J. Mater. Chem. A* **2015**, *3*, 4147−4154.
(33) Bhattacharya, R. N.; Oh, M.-K.; Kim, Y. CIGS-based solar cells prepared from electrodeposited precursor films. *Sol. Energy Mater. Sol. Cells* **2012**, *98*, 198−202.
(34) Oh, Y.; Woo, K.; Lee, D.; Lee, H.; Kim, K.; Kim, I.; Zhong, Z.; Jeong, S.; Moon, J. Role of Anions in Aqueous Sol−Gel Process Enabling Flexible Cu(In,Ga)S2 Thin-Film Solar Cells. *ACS Appl. Mater. Interfaces* **2014**, *6*, 17740−17747.
(35) Choy, K. L. Chemical vapour deposition of coatings. *Prog. Mater. Sci.* **2003**, *48*, 57−170.
(36) Romanyuk, Y. E.; Hagendorfer, H.; Stücheli, P.; Fuchs, P.; Uhl, A. R.; Sutter-Fella, C. M.; Werner, M.; Haass, S.; Stückelberger, J.; Broussillou, C.; Grand, P.-P.; Bermudez, V.; Tiwari, A. N. All Solution-Processed Chalcogenide Solar Cells − from Single Functional Layers Towards a 13.8% Efficient CIGS Device. *Adv. Funct. Mater.* **2015**, *25*, 12−27.
(37) Minami, T.; Nanto, H.; Takata, S. Highly Conductive and Transparent Aluminum Doped Zinc Oxide Thin Films Prepared by RF Magnetron Sputtering. *Jpn. J. Appl. Phys.* **1984**, *23*, L280.
(38) Zhu, X. L.; Wang, Y. M.; Zhou, Z.; Li, A. M.; Zhang, L.; Huang, F. Q. 13.6%-efficient Cu(In,Ga)Se2 solar cell with absorber fabricated by RF sputtering of (In,Ga)2Se3 and CuSe targets. *Sol. Energy Mater. Sol. Cells* **2013**, *113*, 140−143.
(39) Contreras, M. A.; Ramanathan, K.; AbuShama, J.; Hasoon, F.; Young, D. L.; Egaas, B.; Noufi, R. Short Communication: Accelerated Publication: Diode characteristics in state-of-the-art ZnO/CdS/$Cu(In_{1-x}Ga_x)Se_2$ solar cells. *Prog. Photovoltaics* **2005**, *13*, 209−216.
(40) Rincón, C.; Ramírez, F. J. Lattice vibrations of $CuInSe_2$ and $CuGaSe_2$ by Raman microspectrometry. *J. Appl. Phys.* **1992**, *72*, 4321−4324.
(41) Witte, W.; Kniese, R.; Powalla, M. Raman investigations of $Cu(In,Ga)Se_2$ thin films with various copper contents. *Thin Solid Films* **2008**, *517*, 867−869.
(42) Acciarri, M.; Binetti, S.; Le Donne, A.; Vodopivec, B.; Miglio, L.; Marchionna, S.; Meschia, M.; Moneta, R. Cu(In,Ga)Se2 hybrid sputtering/evaporation deposition for thin film solar cells application. In *Photovoltaic Specialists Conference (PVSC), 2012 38th IEEE*, June 3−8, 2012; pp 003087−003091.
(43) Rincón, C.; Wasim, S. M.; Marín, G.; Delgado, J. M.; Huntzinger, J. R.; Zwick, A.; Galibert, J. Raman spectra of the ordered vacancy compounds $CuIn_3Se_5$ and $CuGa_3Se_5$. *Appl. Phys. Lett.* **1998**, *73*, 441−443.
(44) Ahmed, S.; Reuter, K. B.; Gunawan, O.; Guo, L.; Romankiw, L. T.; Deligianni, H. A High Efficiency Electrodeposited Cu2ZnSnS4 Solar Cell. *Adv. Energy Mater.* **2012**, *2*, 253−259.
(45) Contreras, M. A.; Mansfield, L. M.; Egaas, B.; Li, J.; Romero, M.; Noufi, R.; Rudiger-Voigt, E.; Mannstadt, W. Wide bandgap Cu(In,Ga)Se_2 solar cells with improved energy conversion efficiency. *Prog. Photovoltaics* **2012**, *20*, 843−850.

DOI: 10.1021/acsami.5b06666
ACS Appl. Mater. Interfaces 2015, 7, 22497−22503